NASA TECHNICAL NOTE

NASA TN D-3298

NASA TN D-3298

c. 1

TECH LIBRARY KAFB, NM
0130032

LOAN COPY: RETURN
AFWL (WLIL-2)
KIRTLAND AFB, N.M.

A SIMULATION INVESTIGATION OF THE LOADS EXPERIENCED BY A PILOTED LAUNCH VEHICLE

by Robert K. Sleeper

Langley Research Center
Langley Station, Hampton, Va.

NATIONAL AERONAUTICS AND SPACE ADMINISTRATION • WASHINGTON, D. C. • MARCH 1966

TECH LIBRARY KAFB, NM

0130032

A SIMULATION INVESTIGATION OF THE LOADS EXPERIENCED BY A PILOTED LAUNCH VEHICLE

By Robert K. Sleeper

Langley Research Center
Langley Station, Hampton, Va.

NATIONAL AERONAUTICS AND SPACE ADMINISTRATION

For sale by the Clearinghouse for Federal Scientific and Technical Information
Springfield, Virginia 22151 – Price $0.50

A SIMULATION INVESTIGATION OF THE LOADS EXPERIENCED BY A PILOTED LAUNCH VEHICLE

By Robert K. Sleeper
Langley Research Center

SUMMARY

The loads incurred during first-stage piloted flight of a Saturn V type of launch vehicle encountering measured winds have been examined in a fixed-base planar simulation study. The study utilized nonlinear equations of motion with time-varying coefficients and included propellant sloshing dynamics and vehicle flexibility. Three forms of stability augmentation were provided the pilot and the resulting loads from each control mode were compared with the loads developed during control with an attitude-attitude-rate autopilot. The pilot was able to keep the load below that of the reference non-load-relieving autopilot except when rate augmentation was absent. Without rate augmentation, a significant increase in load was incurred.

INTRODUCTION

Astronauts have guided space vehicles in space and during reentry. The value of the pilot's participation during these flight phases has been well demonstrated. Their success has raised the question as to whether the pilot's influence might be extended into the launch phase where only automatic control systems have been used. The use of a pilot in an override capacity in the control loop would provide system redundancy and thereby increase the mission reliability. Also, complete pilot control may be advantageous on future reusable launch vehicles.

To illustrate what a pilot in an override capacity may contribute to mission success, the study of reference 1 examined the mission experience of a manned X-15 airplane which has a control task similar to that of a launch vehicle. In reference 1, a comparison of the actual flights was made with hypothetical flights of an automatically controlled X-15 airplane without control system redundancies. The results showed that, although no actual piloted X-15 flights were lost due to control system failures, 15 of the first 47 flights would have resulted in the loss of the hypothetical automatically controlled vehicle.

The feasibility of using a pilot to control a large launch vehicle was first demonstrated in the ground-based simulation studies reported in reference 2. Centrifuge investigations were also performed in this study and showed that axial accelerations

which arise during launch do not deteriorate the pilot performance as determined on a fixed-base simulation. Presented in reference 3 are the results of simulations and stability studies using the characteristics of a launch vehicle with a Dynasoar type of payload. This study concluded that a pilot can best be used in a back-up capacity. An extensive study with the same configuration was performed in reference 4 and suggested that pilot control may be preferable to automatic control. A simulation study using the properties of the Saturn V vehicle (ref. 5) presented similar conclusions.

These previous studies have emphasized the stability and control aspects of pilot control of launch vehicles, although some load information has been presented. The objective of the present simulation was to determine the effects of pilot control on the loads experienced by a Saturn V type of launch vehicle ascending through winds. The vehicle was simulated throughout first-stage flight by using planar, nonlinear equations-of-motion with time-varying coefficients. Vehicle dynamics were represented by rigid-body, flexible-body, and fuel-sloshing degrees of freedom. Each simulated flight was made through a wind disturbance randomly selected from one synthetic and five measured wind profiles. Pilots guided the vehicle along a specific pitch-attitude program and attempted to minimize lateral accelerations while observing a display consisting of lateral acceleration and attitude. Control of the vehicle was accomplished at three levels of augmentation – full stability augmentation, rate augmentation, and no augmentation. The loads generated for simulated flights at each level of augmentation are compared with the loads produced when the vehicle was flown through the same wind but controlled by a non-load-relieving autopilot.

SYMBOLS

Measurements for this investigation were taken in the U.S. Customary System of Units. Equivalent values are indicated herein in the International System (SI) in the interest of promoting the use of this system in future NASA reports.

a_n rigid-body acceleration normal to vehicle at accelerometer location x_a, ft/sec^2 (m/sec^2)

a_p vehicle attitude gain as a function of time

a_r vehicle attitude-rate gain as a function of time, sec

C_A axial-aerodynamic-force coefficient as a function of Mach number

$C_{b,1}$ bending-moment coefficient associated with normal rigid-body acceleration of vehicle, ft-lb/ft/sec^2 $\left(\text{m-N/m/sec}^2\right)$

$C_{b,2}$ bending-moment coefficient associated with rotational rigid-body acceleration of vehicle as a function of time, ft-lb-sec^2 $\left(\text{m-N-sec}^2\right)$

$C_{b,3}$ bending-moment coefficient associated with flexible-body modal acceleration of vehicle, lb-sec^2 $\left(\text{N-sec}^2\right)$

$C_{b,\alpha}$ bending-moment coefficient associated with aerodynamic angle of attack, ft-lb (m-N)

$C_{m,\alpha}$ aerodynamic-moment coefficient about vehicle center of mass associated with angle of attack, ft-lb (m-N)

$C_{m,\dot{\theta}}$ aerodynamic-moment coefficient about vehicle center of mass associated with rate of rotation of vehicle, ft-lb-sec (m-N-sec)

$C_{N,i}$ distributed normal-aerodynamic-force coefficients located at discrete locations x_i associated with local angle of attack as a function of Mach number

F_A vehicle axial-aerodynamic force, lb (N)

$C_{N,\alpha}$ total normal aerodynamic-force coefficient associated with angle of attack, lb (N)

$C_{N,\dot{\theta}}$ total normal aerodynamic-force coefficient associated with vehicle rotational rate, lb-sec (N-sec)

$C_{q,\alpha}$ total generalized aerodynamic-force coefficient acting in bending mode due to angle of attack, lb (N)

f_e engine frequency, $\frac{\omega_e}{2\pi}$, cps (Hz)

g acceleration of gravity, ft/sec^2 $\left(\text{m/sec}^2\right)$

g_q	vehicle structural modal damping factor
h	altitude, ft (m)
I_{cg}	moment of inertia of vehicle, less engines, about vehicle center of mass as a function of time, slug-ft^2 $(kg\text{-}m^2)$
I_e	equivalent moment of inertia of gimbaled engines about their gimbal point, slug-ft^2 $(kg\text{-}m^2)$
i	summing index
K_τ	reciprocal of linearized engine lag, sec^{-1}
M	Mach number
$M_{b,n}$	bending moment at a point along the vehicle, ft-lb (m-N)
m	vehicle mass, less engine mass, slugs (kg)
m_e	equivalent mass of gimbaled engines, slugs (kg)
m_q	generalized mass of bending mode, slugs (kg)
m_1, m_2	propellant sloshing masses as functions of time, slugs (kg)
N	filtered Gaussian noise, ft/sec (m/sec)
q	generalized coordinate of bending mode, ft (m)
S_o	aerodynamic-load reference area, 855.3 ft^2 $(79.5m^2)$
s	Laplace transform complex variable, sec^{-1}
T	total thrust of engines, lb (N)
t	time, sec
V_m	vehicle velocity, ft/sec (m/sec)

$V_{m,w}$	vehicle velocity relative to wind, ft/sec (m/sec)
V_w	wind velocity (horizontal) as a function of altitude, ft/sec (m/sec)
V_x	component of center-of-gravity velocity vector along X-axis, ft/sec (m/sec)
V_y	component of center-of-gravity velocity vector along Y-axis, ft/sec (m/sec)
x	body-fixed longitudinal-coordinate with origin at engine gimbal, ft (m)
x_1, x_2	locations of sloshing mass along vehicle longitudinal axis as a function of time, ft (m)
x_a	location of accelerometer along vehicle longitudinal axis, ft (m)
$x_{b,n}$	longitudinal position where bending moment is computed, ft (m)
x_{cg}	longitudinal position of vehicle center of mass as a function of time, ft (m)
x_e	distance of engine center of mass from engine gimbal, ft (m)
x_i	longitudinal positions of concentrated normal aerodynamic forces, ft (m)
y	body-fixed coordinate normal to undeformed vehicle center line, ft (m)
α	rigid-body angle of attack, rad
α_w	wind-induced rigid-body angle of attack, rad
δ	gimbaled engine deflection angle relative to deflected vehicle center line, rad
δ_c	command gimbaled engine deflection angle, rad
$\overline{\delta}$	piloted roll command, rad
ζ_1, ζ_2	viscous damping ratios of sloshing mass motion

ζ_e	viscous damping ratio of engine motion
ζ_p	viscous damping ratio of rigid-body pitch mode
θ	vehicle attitude relative to horizontal, rad
θ_c	vehicle attitude command, rad
θ_ϵ	vehicle attitude error, rad
$\overline{\theta}$	roll variable, rad
λ_1, λ_2	propellant-slosh coordinates measured from deflected vehicle center line, ft (m)
$\rho(h)$	atmospheric density as a function of altitude, slugs/ft^3 (kg/m^3)
ϕ	modal deflection of vehicle center line normalized to unity at gimbal point, x = 0
ϕ_1, ϕ_2	modal deflection at sloshing mass position x_1 and x_2, respectively, as a function of time
ϕ_g	modal deflection (normalized to unity) at gimbal point, x = 0
ϕ_i	modal deflection at normal aerodynamic force location x_i
ϕ_p	modal deflection at attitude gyro position as a function of time
ϕ_r	modal deflection at attitude rate gyro position as a function of time
ω	transfer-function frequency, rad/sec
ω_e	circular frequency of engine, rad/sec
ω_p	rigid-body pitch frequency, rad/sec

ω_q uncoupled natural frequency of bending mode as a function of time, rad/sec

ω_1, ω_2 uncoupled natural sloshing frequencies, rad/sec

A dot over a variable indicates differentiation with respect to time.

A prime with a variable indicates the slope of the variable with respect to the longitudinal coordinate x.

DESCRIPTION OF SIMULATION

This study was conducted with a simulator composed of a cockpit coupled with two conventional analog computers. The cockpit contained both a display, which presented vehicle normal acceleration and attitude to the pilot, and a pencil type of two-axis controller. During the 150.45-second simulation, the pilot controlled the vehicle with one of three levels of control-system augmentation as it ascended through winds. The vehicle loads resulting from flights using each of these control modes were compared with loads produced during autopilot control. Although the dynamic equations were valid for the pitch plane only, the pilot was also required to control a roll disturbance continuously. This control task was required to give the pilot a more realistic work load. The pilots' objective was to minimize loads in the high dynamic-pressure region as well as to achieve minimum attitude error at first-stage burnout.

The simulation featured characteristics of a large launch vehicle similar to the Saturn V as its mathematical model. Flexibility and sloshing dynamics were incorporated into nonlinear equations of motion with time-varying coefficients and Mach number dependent aerodynamics. Arbitrarily selected wind profiles were used to disturb the vehicle during the simulated flights.

Description of Cockpit

Display.- The cockpit display shown in figure 1 consisted of an attitude indicator, an acceleration indicator (rate meter), a time indicator, and indicator lights.

At the lower right of the display, the all-attitude indicator, which is capable of displaying seven variables, is shown; however, only three of its presentations were required in the present study. The current attitude of the vehicle was displayed on the rotating sphere by a fixed pointer and the programed attitude was superimposed on the sphere to the same scale by the translating flight-director needle. Any error was presented as the distance between the needle and the fixed reference. Thus, a pursuit type of display was presented to the pilot who was required to null or superimpose the flight-director needle

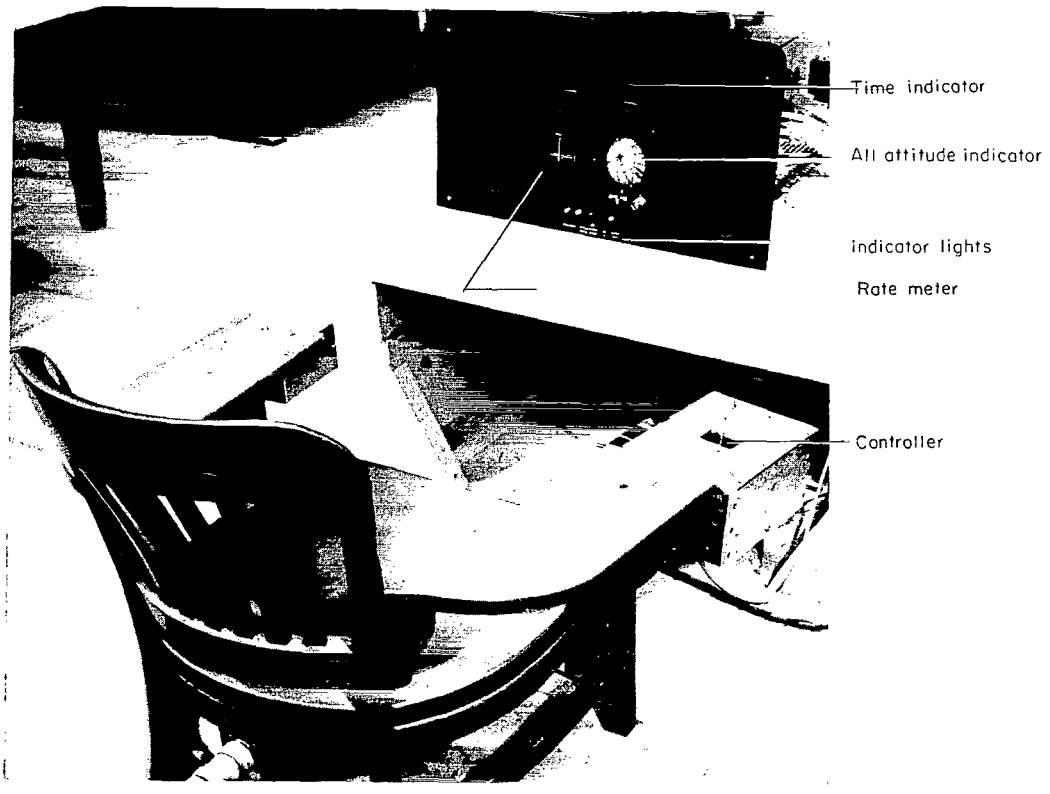

Figure 1.- Simulator cockpit. L-64-11524.1

on the fixed attitude reference for attitude control. This presentation was used to negotiate pitchover and aline the vehicle preparatory to encountering the high load region. After passing through the high dynamic-pressure region, it was used to arrest attitude excursions in preparation for burnout.

Because the analysis was conducted only in the pitch plane, a roll task was included in the simulation to provide a more realistic work load for the pilot. This roll disturbance was presented to the pilot by rotation of the sphere in the all-attitude indicator. It consisted of a disturbed, linear, second-order, damped oscillatory system with constant coefficients which the pilot was required to null continuously. The disturbance supplied was proportional to the wind velocity; however, to disguise the wind in the response displayed to the pilot, fluctuations in the wind velocity were added to the roll disturbance in the form of filtered Gaussian noise. The basic equation to be zeroed was

$$\ddot{\overline{\theta}} + 1.886\dot{\overline{\theta}} + 1.579\overline{\theta} = 1.528\overline{\delta} + K\left(V_W + N\right)$$

where $\bar{\delta}$ is the piloted roll command, K is a suitable gain, and N is the filtered Gaussian noise. This relation presented to the pilot a 0.7 critically damped oscillatory system with a natural frequency of 0.2 cps (0.2 Hz). The noise, which was generated at frequencies up to 32 cps (32 Hz) by a Gaussian noise generator, was filtered by the expression $1/(0.25s + 1)$.

The predominant contributor to the bending moment is the aerodynamic load which results when the vehicle develops an angle of attack. An instrument to measure this quantity is complex; however, from theoretical considerations, an accelerometer may be made to approximate an angle-of-attack sensor when the accelerometer is located at the instantaneous center of rotation. This center of rotation is defined as the longitudinal position about which the vehicle rotates due to the control force in the absence of aerodynamic forces. This arrangement was recommended in reference 4. Thus, an ideal accelerometer, indicating rigid-body acceleration, was used to display loads information to the pilot. The right-hand needle of the meter shown at the lower left (fig. 1) was used for this presentation. Its motion was vertical and indicated the normal acceleration being developed. A full-scale reading corresponded to 0.3g.

The approximate transfer functions of the indicators are included in appendix A.

The upper meter shown in the display was used to present elapsed time to the pilot. Events of start, pitchover, approximate maximum dynamic pressure, and burnout were designated along the scale to enable the pilots to anticipate significant phases of the flight. In addition, lights were used to supplement the time indicator by indicating time for pitchover, the high dynamic-pressure region (45 to 94 sec), and burnout.

Controller.- The pilot controlled a linear pencil type of controller (shown in fig. 1) which had a small dead band to facilitate centering via an indicator. Other characteristics of the controller are presented in appendix A.

Equations of Motion

Continuous equations of motion, simplified from equations developed in reference 6, were used in the simulation and are presented in this section. These planar equations used body-fixed coordinates to simplify expressions for fuel sloshing and flexible-body motion relative to the vehicle. In addition, the engine dynamics were assumed to be described by a linear transfer function, and the vehicle was acted upon by aerodynamic forces which were functions of Mach number. Also included in this section are the bending-moment equation and the rigid-body-acceleration equation used to display the load information to the pilot. A sketch of the coordinate system is shown in figure 2.

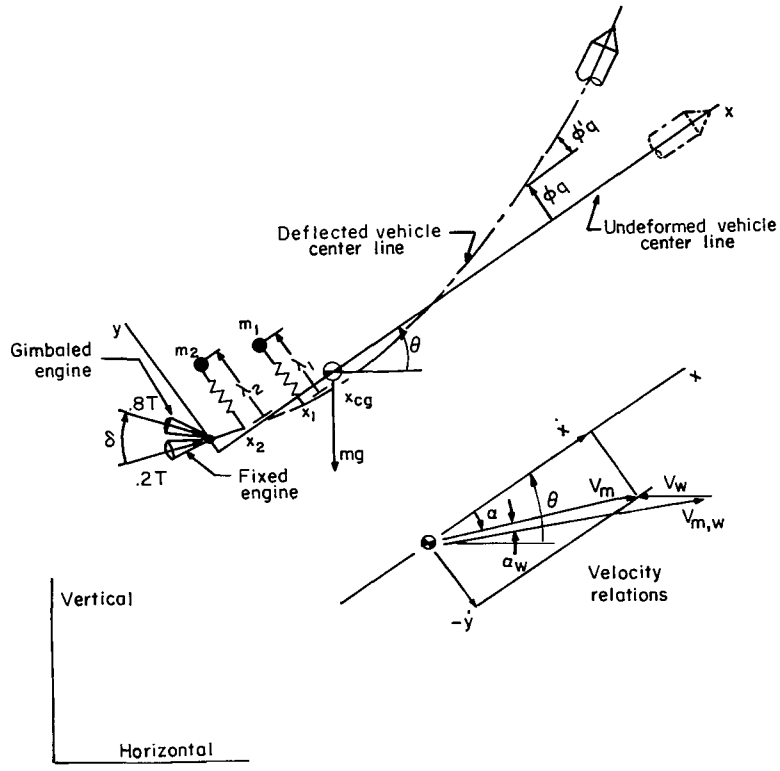

Figure 2.- Coordinate system.

Rigid-body motion.- The simplified nonlinear rigid-body motion equations used in the simulation are as follows:

Axial equation –

$$\dot{V}_x = \dot{\theta} V_y - g \sin\theta + \frac{1}{m}\left(T - F_A\right)$$

Normal equation –

$$\dot{V}_y = -\dot{\theta} V_x - g \cos\theta + \frac{1}{m}\left[T\left(\phi'_g q - 0.8\delta\right) + C_{N,\alpha}\left(\alpha + \alpha_w\right) + C_{N,\dot{\theta}}\dot{\theta} - m_1\ddot{\lambda}_1 - m_2\ddot{\lambda}_2 - m_e x_e \ddot{\delta}\right]$$

Pitching equation –

$$\ddot{\theta} = \frac{1}{I_{cg}}\left[T x_{cg}\left(0.8\delta - \phi'_g q\right) - Tq + C_{m,\alpha}\left(\alpha + \alpha_w\right) + C_{m,\dot{\theta}}\dot{\theta} - m_1\left(x_1 - x_{cg}\right)\ddot{\lambda}_1 - m_2\left(x_2 - x_{cg}\right)\ddot{\lambda}_2 + \dot{V}_x\left(m_1\lambda_1 + m_2\lambda_2\right) + \left(I_e + m_e x_e x_{cg}\right)\ddot{\delta}\right]$$

where the symbols q, δ, λ_1, and λ_2 are associated with the flexibility, engine deflection, and the two sloshing coordinates, respectively. Engine inertia terms have been included to simulate more closely the control behavior. The factor 0.8 appears in the normal and pitching equations since only 80 percent of the thrust was available for control.

Flexible-body motion.- The flexible-body motion of the vehicle was represented by a free-free bending mode of oscillation which included small viscous structural damping and time-varying effects attributed to propellant ullage. Its motion was governed by the following equation:

$$\left(\ddot{q} + \omega_q g_q \dot{q} + \omega_q^2 q\right) = \frac{1}{m_q}\Big[T\phi_g\left(\phi_g' q - 0.8\delta\right) + C_{q,\alpha}\left(\alpha + \alpha_w\right) - \phi_1 m_1 \ddot{\lambda}_1$$

$$- \phi_2 m_2 \ddot{\lambda}_2 + \left(I_e \phi_g' - m_e x_e \phi_g\right)\ddot{\delta}\Big]$$

Propellant sloshing motion.- Two linear spring-mass systems with small viscous damping were used to represent the motion of the sloshing fuel and oxidizer. These equations are

$$\left(\ddot{\lambda}_1 + 2\omega_1 \zeta_1 \dot{\lambda}_1 + \omega_1^2 \lambda_1\right) = -\left[\left(\dot{V}_y + \dot{\theta} V_x + g \cos\theta\right) + \left(x_1 - x_{cg}\right)\ddot{\theta} + \phi_1 \ddot{q}\right] \quad .$$

$$\left(\ddot{\lambda}_2 + 2\omega_2 \zeta_2 \dot{\lambda}_2 + \omega_2^2 \lambda_2\right) = -\left[\left(\dot{V}_y + \dot{\theta} V_x + g \cos\theta\right) + \left(x_2 - x_{cg}\right)\ddot{\theta} + \phi_2 \ddot{q}\right]$$

To account for propellant ullage, the fixed propellant mass and sloshing mass and their locations varied with time. In addition, the sloshing frequencies were assumed to be functions of time and axial acceleration.

Engine dynamics.- All the gimbaling engines were dynamically represented by a single third-order differential equation, composed of oscillatory and lag responses as follows

$$\dddot{\delta} + \left(K_T + 2\zeta_e \omega_e\right)\ddot{\delta} + \left(2K_T \zeta_e \omega_e + \omega_e^2\right)\dot{\delta} + K_T \omega_e^2 \delta = K_T \omega_e^2 \delta_c$$

Aerodynamic forces.- In addition to disturbances imposed by the engines, the vehicle was influenced by an aerodynamic loading. These loads consisted of forces and moments which are represented by four concentrated normal aerodynamic loads located along the vehicle and were chosen to represent the total aerodynamic normal force and pitching moment about the center of gravity of the vehicle. The normal loads were

expressed by Mach number-dependent aerodynamic coefficients, $C_{N,i}$, which were linear with the local angle of attack.

The total aerodynamic-load coefficients associated with the rigid-body angle of attack were expressed in terms of the concentrated aerodynamic coefficients by the following equations:

Rigid-body aerodynamic force and moment –

$$C_{N,\alpha} = \frac{1}{2}\rho V_{m,w}^2 S_o \sum_{i=1}^{4} C_{N,i}$$

$$C_{m,\alpha} = \frac{1}{2}\rho V_{m,w}^2 S_o \sum_{i=1}^{4} C_{N,i}\left(x_i - x_{cg}\right)$$

Flexible-body aerodynamic force –

$$C_{q,\alpha} = \frac{1}{2}\rho V_{m,w}^2 S_o \sum_{i=1}^{4} C_{N,i}\phi_i$$

where the mode shape was assumed to be constant at its value near the time of maximum dynamic pressure. Also quasi-steady aerodynamic effects due to $\dot{\theta}$ which varied with Mach number were included in the rigid-body loads. These expressions for the total rigid-body load coefficient associated with the vehicle rate of rotation are

$$C_{N,\dot{\theta}} = -\frac{1}{2}\rho V_{m,w} S_o \sum_{i=1}^{4} C_{N,i}\left(x_i - x_{cg}\right)$$

$$C_{m,\dot{\theta}} = -\frac{1}{2}\rho V_{m,w} S_o \sum_{i=1}^{4} C_{N,i}\left(x_i - x_{cg}\right)^2$$

The axial force is given by

$$F_A = \frac{1}{2}\rho V_{m,w}^2 S_o C_A$$

The axial force varied with Mach number but was assumed to be independent of angle of attack.

The bending-moment coefficient due to the aerodynamic force which was used in the computation of the bending moment presented in a subsequent section is given by

$$C_{b,\alpha} = \frac{1}{2}\rho V_{m,w}^2 S_o \sum_i C_{N,i}\left(x_i - x_{b,n}\right)$$

where only the loads forward of the point of interest $\left(x_{b,n}\right)$ are considered.

Variations in atmospheric density ρ and sonic velocity with altitude were programed into the simulation.

Normal acceleration.- The equation for the normal acceleration is

$$a_n = \left(\dot{V}_y + \dot{\theta} V_x + g \cos \theta\right) + \left(x_a - x_{cg}\right)\ddot{\theta}$$

In order to produce a signal proportional to the angle of attack, the accelerometer was located near the instantaneous center of rotation of the vehicle. In addition, flights were made with a forward sensor location which indicated the effect of this position on the loads.

Bending moment.- The bending moment was computed at one location along the vehicle. Its position was chosen forward of the sloshing propellant tanks in the region where the bending moment was large. The equation has been expressed in terms of the aerodynamic loading and the resulting vehicle lateral acceleration forward of the point of interest. The equation for the bending moment used is

$$M_{b,n} = C_{b,1}\left(\dot{V}_y + \dot{\theta} V_x + g \cos \theta\right) + C_{b,2} \cdot \ddot{\theta} + C_{b,3}\ddot{q} + C_{b,\alpha} \cdot \left(\alpha + \alpha_w\right)$$

Because the mass forward of the propellant tanks does not change, the coefficient $C_{b,1}$ associated with the rigid-body lateral acceleration was constant and the coefficient $C_{b,2}$ associated with the rigid-body rotational acceleration was a function of the time-varying center of gravity. In addition, the coefficient $C_{b,3}$ associated with the flexible-body modal acceleration was assumed constant, that is, the mode shape was fixed at the time that maximum dynamic pressure occurred. The aerodynamic coefficient $C_{b,\alpha}$ associated with the angle of attack was a function of Mach number and dynamic pressure.

Description of Control Systems

The four control configurations used in the simulation consisted of the automatic control system and three piloted control modes: (1) stability augmented, (2) rate augmented, and (3) no augmentation. The automatic control system was used to provide a standard of reference for comparison with the piloted responses. It also supplied the augmentation for the piloted control modes since these modes were established by deleting, in turn, the pitch-program command, the attitude feedback, and the attitude-rate feedback.

Automatic control system.- An attitude-attitude-rate autopilot with ideal sensors was assumed for the automatic control system. A schematic of the control system is shown in figure 3(a); the control equation is

$$\theta_\epsilon = -a_p\left(\theta - \theta_c + \phi_p' q\right) - a_r\left(\dot{\theta} + \phi_r' \dot{q}\right)$$

where control gains a_p and a_r were assumed to be linear functions of time. Control gains alone could not stabilize the flexible vehicle and a lag filter was required in the forward loop.

Stability-augmented control mode.- In the stability-augmented control mode (fig. 3(b)) the pilot utilized all the autopilot feedback and merely replaced a summing device. His task was to maintain the pitch-attitude time history which was displayed to him as an attitude error. However, in order to permit controller commands about its center, an integrator was required in the controller circuitry and introduced some lag into the system.

Rate-augmented control mode.- As illustrated in figure 3(c), the rate-augmented control mode was the same as the stability-augmented mode except the integrator was removed from the controller and only the attitude-rate was retained in the feedback, making the system statically (aerodynamically) unstable.

No-augmentation control mode.- In the control mode with no augmentation, as shown in figure 3(d), the remaining rate augmentation (and all structural feedback) was removed from the control system, thereby making the vehicle more unstable. In general, the pilot did not want a filter in the control system because of the lag it introduces; however, such a filter reduces the high-frequency content of the pilot's command signal and was retained in this mode.

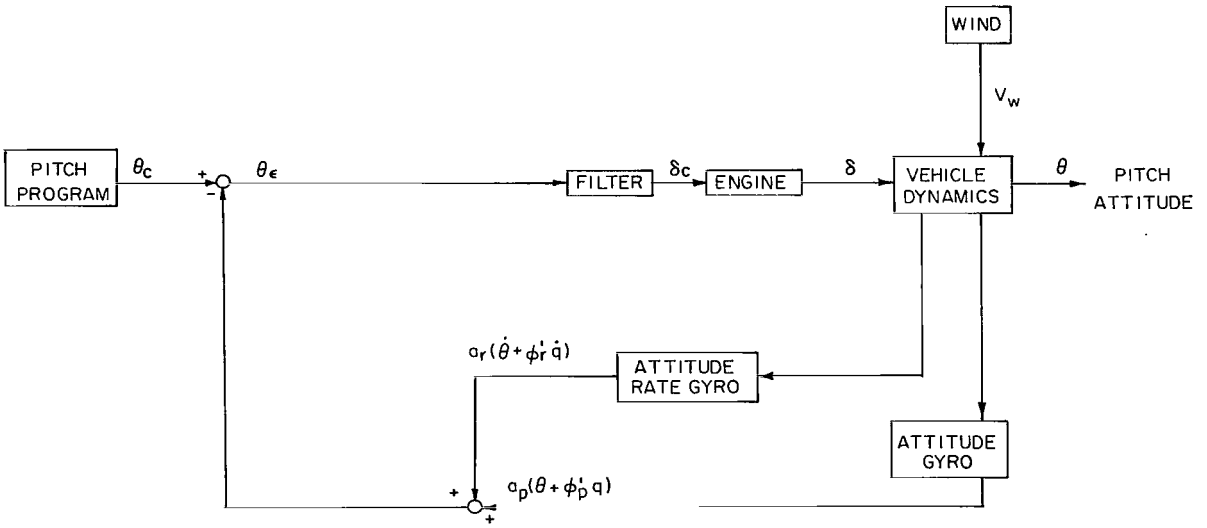

(a) Autopilot control system.

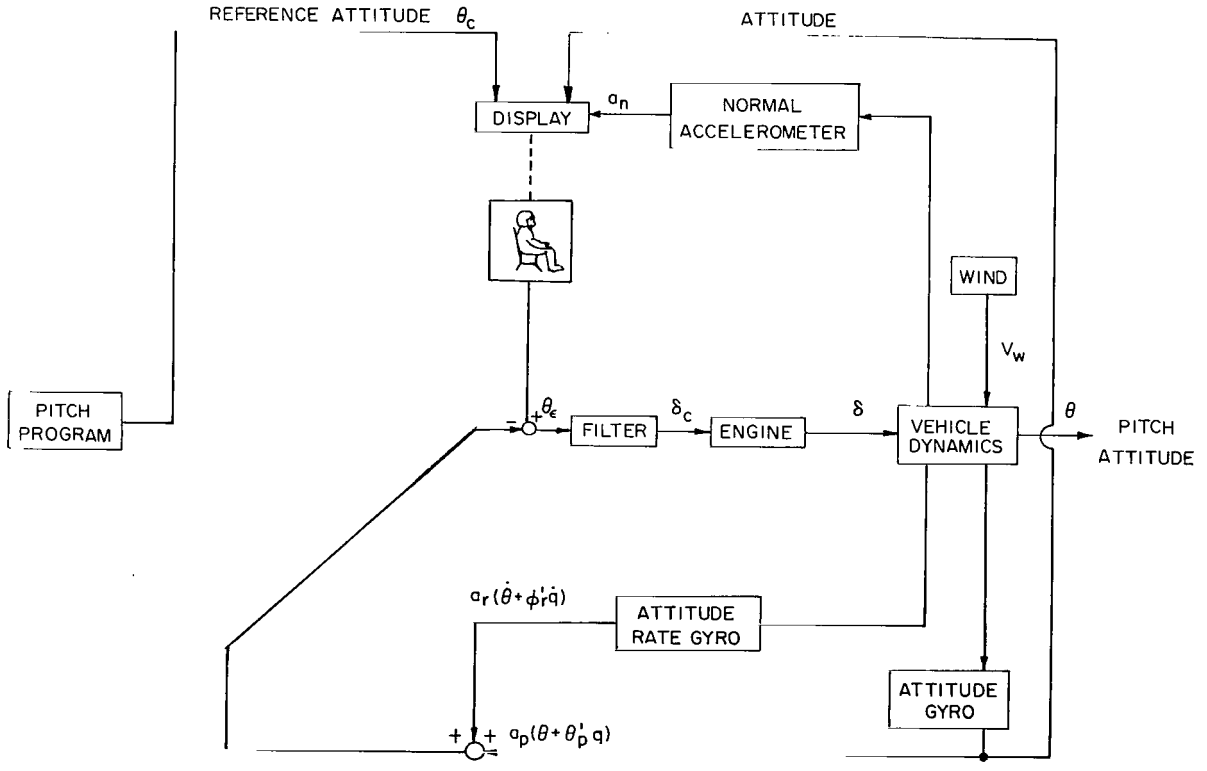

(b) Stability augmented control mode.

Figure 3.- Control systems.

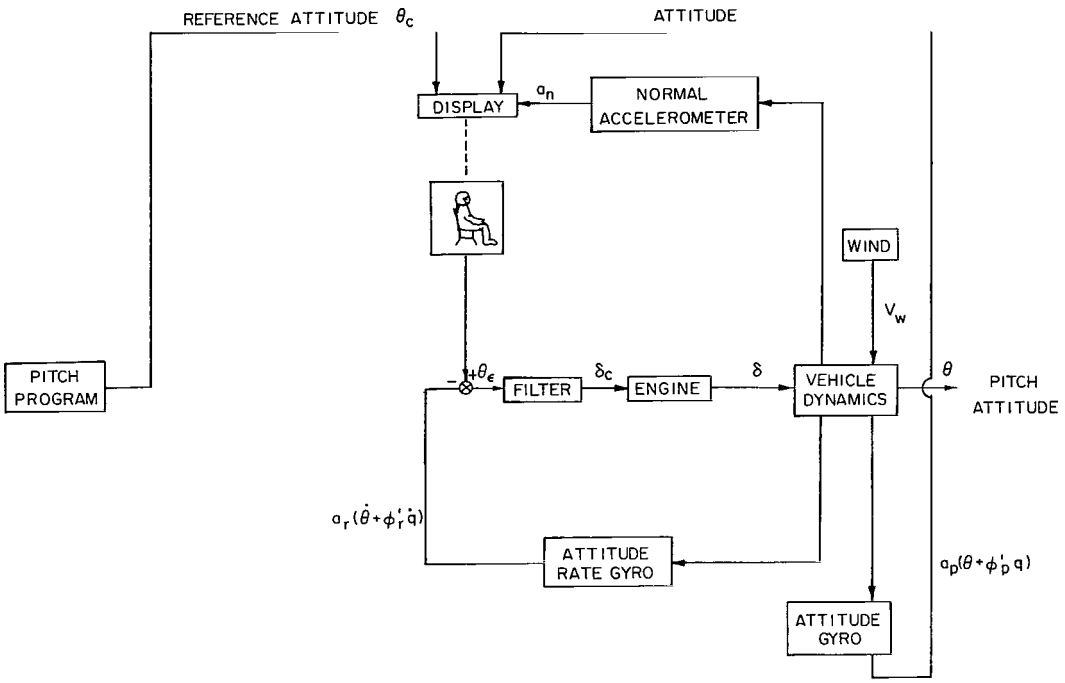

(c) Rate augmented control mode.

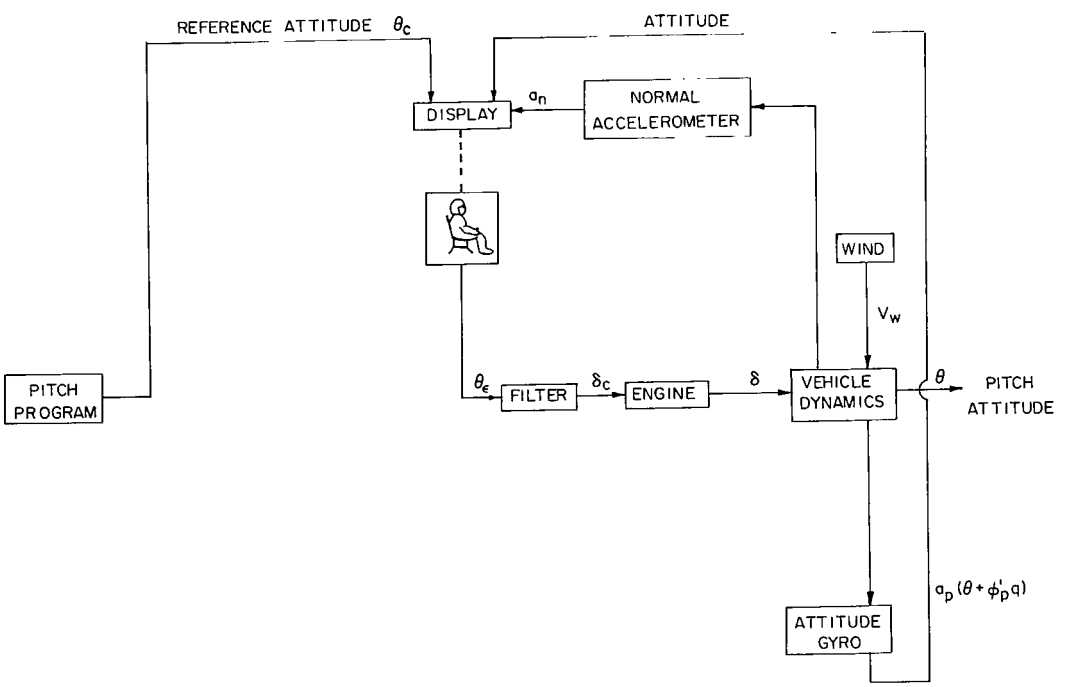

(d) Control mode with no augmentation.

Figure 3.- Concluded.

Vehicle Characteristics

The launch-vehicle configuration used for this investigation is shown in figure 4. Its properties were similar to those of the Saturn V vehicle. It had a 1.25 thrust-to-weight ratio at lift-off with thrust provided by four controllable gimbaling engines plus one fixed engine the thrust of which terminated automatically 6 seconds prior to burnout of the gimbaling engines. Each engine developed 1.5×10^6 lb (6.68×10^6 N) of thrust at sea level and the thrust increased with altitude. The vehicle experienced a maximum dynamic pressure of 670 psf (32 100 N/m^2) near the middle of its first-stage flight and attained an approximate velocity of 7500 fps (2290 m/s) at an altitude of 237 000 ft (72 300 m) at first-stage burnout.

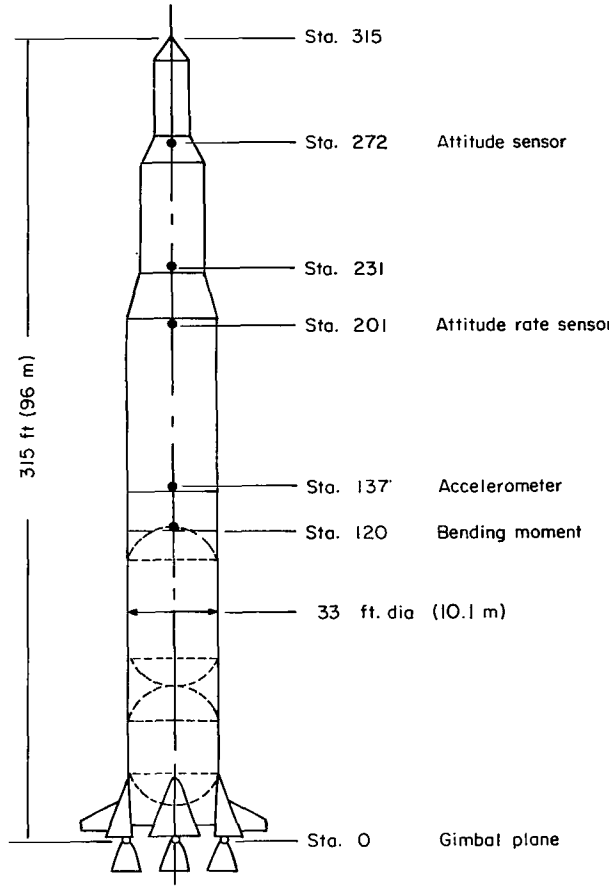

Figure 4.- Simulation vehicle configuration.

Vehicle description.- The basic properties of the simulated vehicle are given in appendix B, and the vehicle moment of inertia is presented in figure 5 as a function of time.

The normalized free-free bending mode, representing the flexible-body motion, is given in figure 6 for three flight times. The structural damping factor g_q was assumed to be 0.01 and the first bending-mode frequency when all the degrees of freedom were coupled together, was nearly constant at 1.2 cps (1.2 Hz).

The sloshing dynamics included viscous-damping ratios (ζ_1, ζ_2) of 0.005 and initial sloshing masses of 12 400 and 8800 slugs (181 000 and 128 000 kg) for the forward and aft tanks, respectively. The coupled sloshing frequencies were near 0.4 cps (0.4 Hz) from both tanks during much of the flight.

The third-order engine representation contained a 0.05-second lag $(K_T = 20 \text{ sec}^{-1})$ and an oscillatory frequency f_e of 8.14 cps (8.14 Hz) with 0.02 critical damping.

The accelerometer position corresponding to the instantaneous center of rotation of the vehicle was located at station 137. Additional flights were conducted with the accelerometer located at station 231.

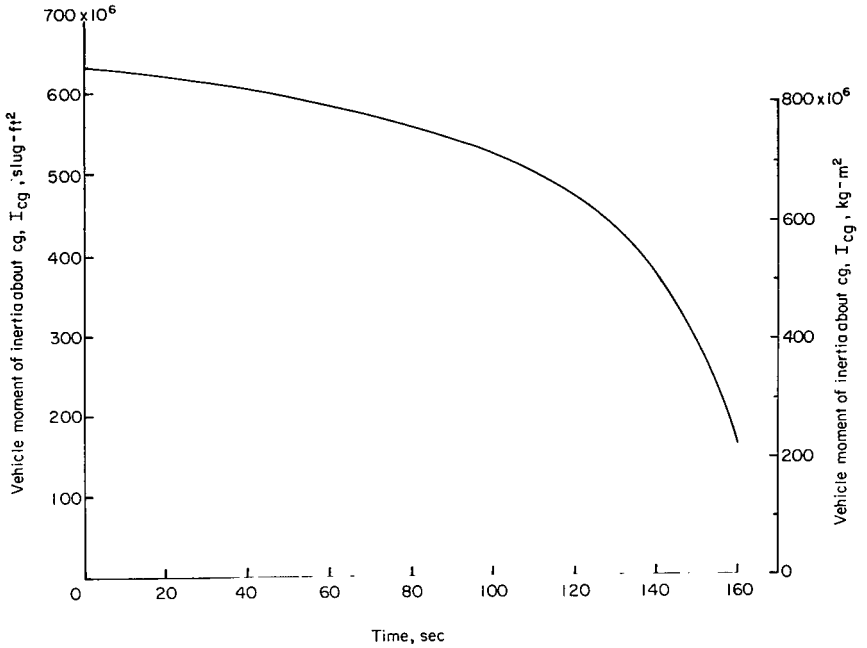

Figure 5.- Vehicle moment of inertia.

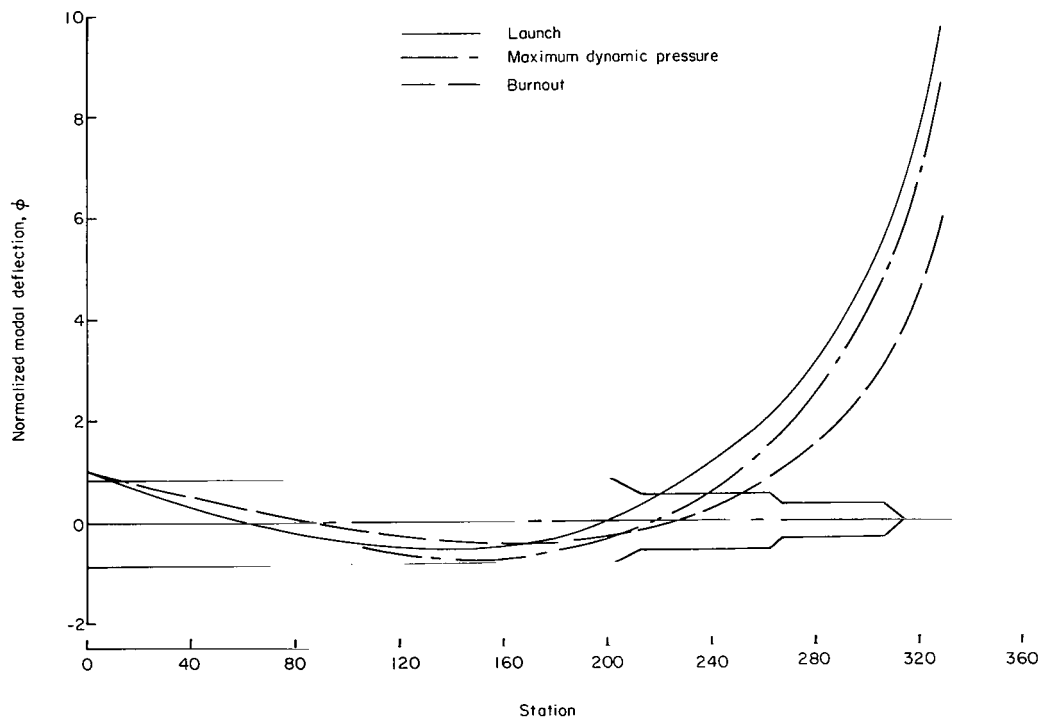

Figure 6.- Mode shapes for three flight times.

Aerodynamic properties.- The Mach number variation of the concentrated aerodynamic normal-force coefficients $C_{N,i}$, which were used to compute the aerodynamic load, and of the axial-force coefficient C_A, are presented in figures 7 and 8. These

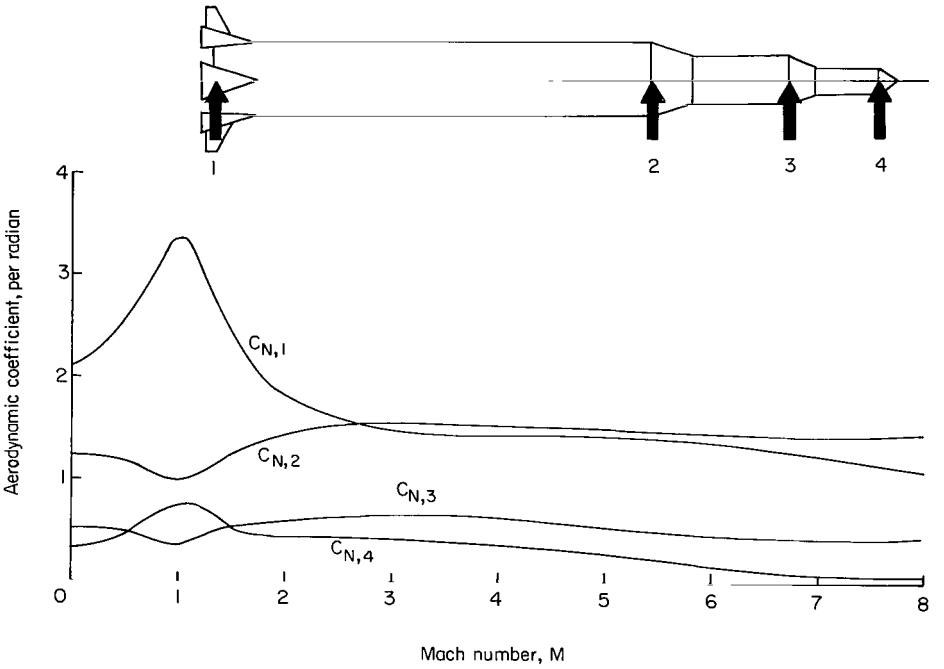

Figure 7.- Variation of concentrated aerodynamic normal-force coefficients with Mach number.

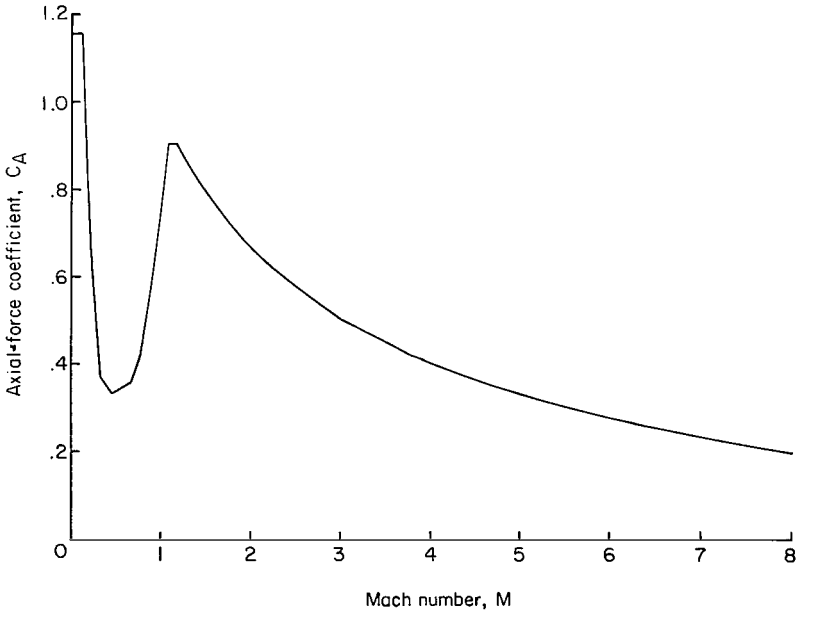

Figure 8.- Variation of axial-force coefficient with Mach number.

coefficients are based on a reference area of 855.3 sq ft (79.5 m^2) and are for a Saturn V type of vehicle. The concentrated normal-force coefficients were also used to derive the aerodynamic bending-moment coefficient, shown in figure 9, for use in the computation of $C_{b,\alpha}$.

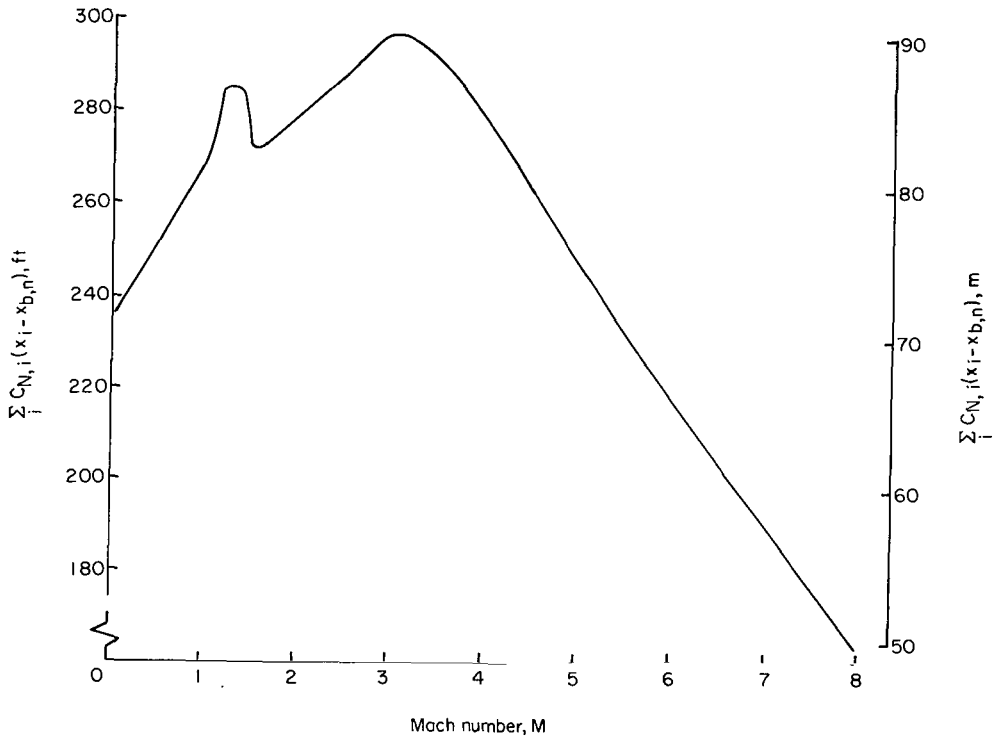

Figure 9.- Bending-moment aerodynamic-coefficient parameter.

A typical no-wind dynamic-pressure time history is shown in figure 10. Although the time history exhibits no initial dynamic pressure, an initial velocity was inserted into the simulation to overcome an indeterminant angle-of-attack condition. A velocity of 9 fps (2.7 m/s) was used.

Control system.- Attitude and attitude-rate sensors located at stations 272 and 201, respectively, were used with control gains of

$$a_p = 0.501 - 0.002014t$$

and

$$a_r = 1.039 - 0.00449t$$

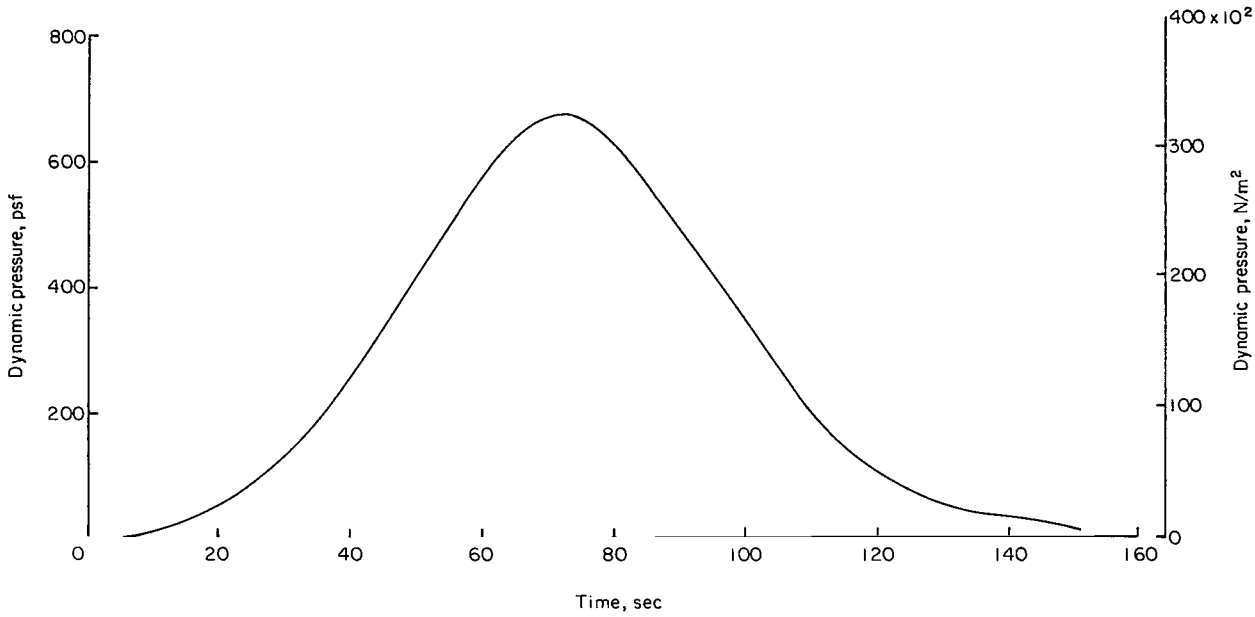

Figure 10.- Typical no-wind dynamic-pressure time history.

in the control system. To stabilize the flexible-body motion, a simple lag filter with a break frequency at 0.239 cps (0.239 Hz) was used in the forward loop of the autopilot. A rigid-body control frequency of approximately 0.12 cps (0.12 Hz) with 0.35 critical damping resulted.

In order to improve piloted response characteristics in the rate-augmented and no-augmentation modes, the filter roll-off frequency was changed from 0.239 to 0.318 cps (0.239 to 0.318 Hz).

The preprogramed command attitude supplied to the automatic control system (fig. 11) produced a trajectory with a minimum angle of attack through the high dynamic-pressure region in the absence of a wind. The attitude which resulted when the vehicle was automatically controlled was then programed for the piloted flights.

Wind Disturbances

The wind profiles used in this investigation are shown in figure 12. Each profile is plotted as horizontal wind velocity as a function of altitude. The winds are numbered in order of increasing maximum velocity. Five of these winds (1, 2, 3, 4, and 6) represent actual wind profiles measured at Wallops Island, Virginia. Wind 5 is a commonly used synthetic wind profile from reference 7. As seen from the data in figure 12, five of the winds have their maximum velocities at an altitude of about 35 000 ft (10 700 m). This altitude is in the region of maximum dynamic pressure for the vehicle used in this study.

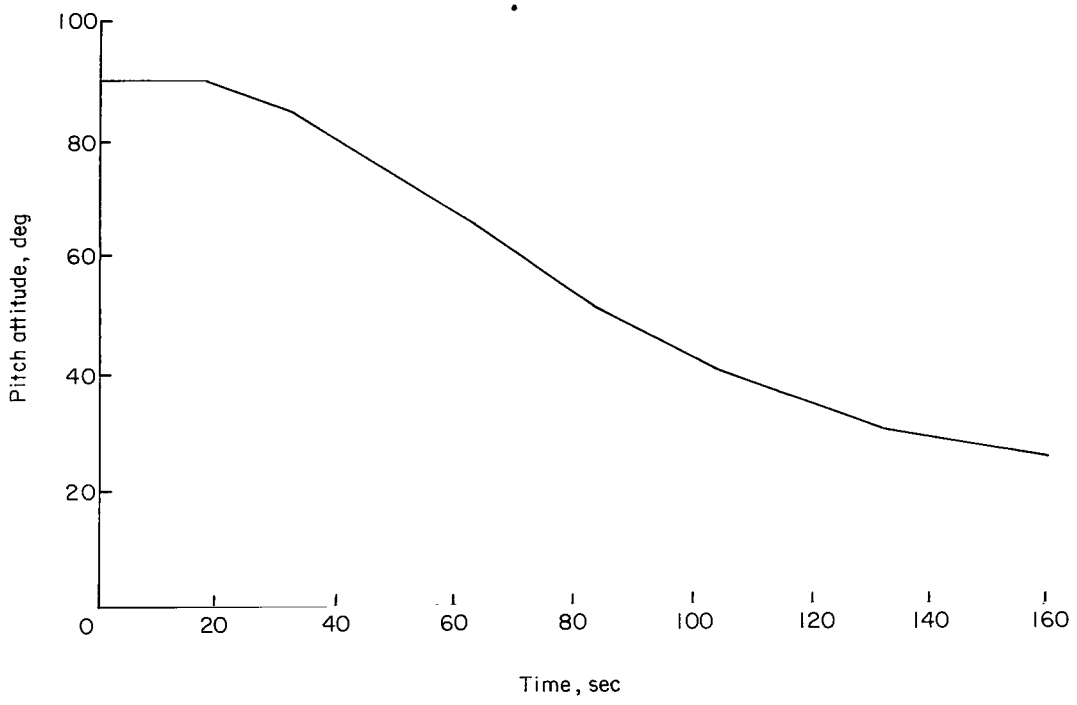

Figure 11.- Programed command attitude.

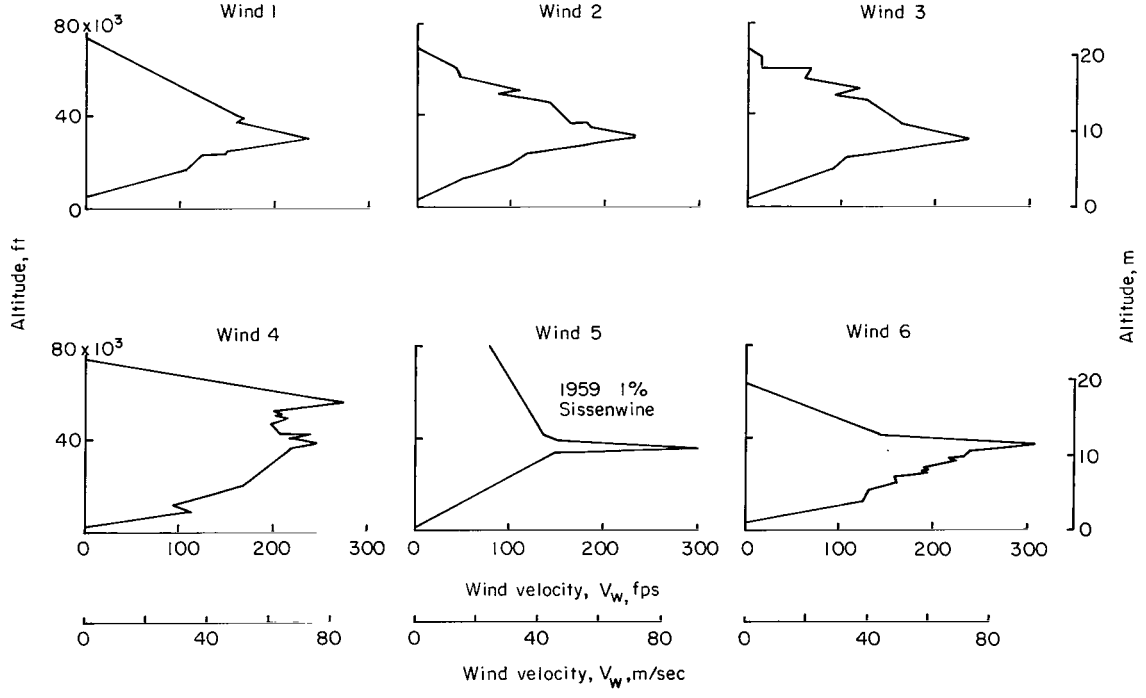

Figure 12.- Wind profiles used in simulation.

The remaining wind (wind 4) has its maximum velocity at an altitude of about 55 000 ft (16 800 m). However, a second wind-velocity peak on this particular profile at 35 000 ft is only slightly lower than the peak at 55 000 ft. All six winds would be classed as relatively severe for the peak velocities are within the 95 percentile category for annual winds at Cape Kennedy (ref. 8).

"Headwinds" were considered more severe and were generally used; however, the wind was reversed occasionally to minimize pilot learning. In addition, flights without any wind disturbance were also scheduled. The wind condition was arbitrarily selected for each flight.

The equation used to couple the wind into the aerodynamics is (see fig. 2)

$$(\alpha + \alpha_w) = \tan^{-1}\left(-\frac{V_y}{V_x}\right) + \sin^{-1}\frac{V_w}{V_{m,w}}\sin(\theta - \alpha)$$

Procedure

When the pilot had familiarized himself with the simulation procedures, one of the wind conditions, which was randomly selected and unknown to the pilot, was fed into the computer. The pilot was informed that his task was to reduce the load and arrest the attitude error prior to burnout. He was required to control attitude before and shortly after negotiating pitchover. As the high load region approached, that is, when the high-dynamic-pressure light became illuminated, the pilot was instructed to maintain low acceleration (to minimize loads) and when the light was extinguished he was to arrest the error and damp any motion prior to burnout. After each flight, which also required the pilot to null continuously a roll disturbance, the pilot rated the run using a Cooper rating schedule (ref. 9).

RESULTS AND DISCUSSION

In this study pilots controlled a large launch vehicle through its first-stage flight. The maximum loads produced in the simulation flights by Langley test pilots were examined in each control mode and compared with loads produced by an autopilot-controlled vehicle ascending through the same wind. In addition, pilot ratings were recorded to present the pilot's evaluation of the control modes.

Piloted flights were conducted with the load-sensing accelerometer located at two stations and a comparison of the results at both locations showed that little difference occurred in either the load and/or the pilot rating for these two accelerometer locations. Consequently, results from all the simulated flights are included without reference to the accelerometer location.

The pilots were required to arrest the motion and error of the vehicle as the flight terminated to conform with typical flight constraints. During the simulated flights, average values for the pitch rate and pitch error of 1.1 deg/sec and 1 degree, respectively, were recorded. Since these were low values, it was concluded that staging requirements could be met. No further evaluation of these end conditions was performed.

Effect of Control Modes

Three piloted modes of control were used in the simulation: (1) stability augmented, (2) rate augmented, and (3) no augmentation. The stability-augmentation mode contained all the augmentation common to the autopilot; therefore, it was a stable configuration. Its response was characterized by a low control frequency $\left(0.75 \leqq \omega_p \leqq 0.98 \text{ rps}\right)$ with low damping $\left(0.29 \leqq \zeta_p \leqq 0.44\right)$ and a slowly converging response associated with the drift. In the rate-augmented mode, the vehicle was slightly unstable because the attitude feedback was absent; however, because the integration in the controller was not required, control and handling qualities in this mode were not appreciably degenerated although increased pilot attention was required. The no-augmentation mode contained a more unstable oscillatory response than the rate-augmented mode and, in addition, contained a slowly converging characteristic response. The pilots noted a marked deterioration in controllability in this mode and generally reported that control was marginal. They frequently relinquished the load-minimizing task to monitor attitude in order to retain control of the vehicle.

Piloted Response and Loads

A piloted time history of a demonstrative flight without augmentation and the corresponding autopilot response are shown for comparison in figure 13. The time history includes the disturbing wind (wind 1), the rigid-body attitude error, angle of attack, the acceleration measured by the accelerometer, and the bending moment. As the flight progressed, the attitude error shows that the pilot negotiated pitchover satisfactorily but encountered difficulty in arresting the attitude error before the load-indicating acceleration began to build up. Therefore, at this time, the pilot was required to reduce the acceleration to an acceptable amount without regard to the increasing attitude error. When the pilot finally did reduce the acceleration, he returned to the error-nulling task for the duration of the first-stage flight.

Slight oscillations appearing in the acceleration and bending-moment time histories were due to elastic-body response. Although sloshing effects are apparent in the acceleration time histories, they were not discernible in the load time histories, a result which has also been reported in reference 10.

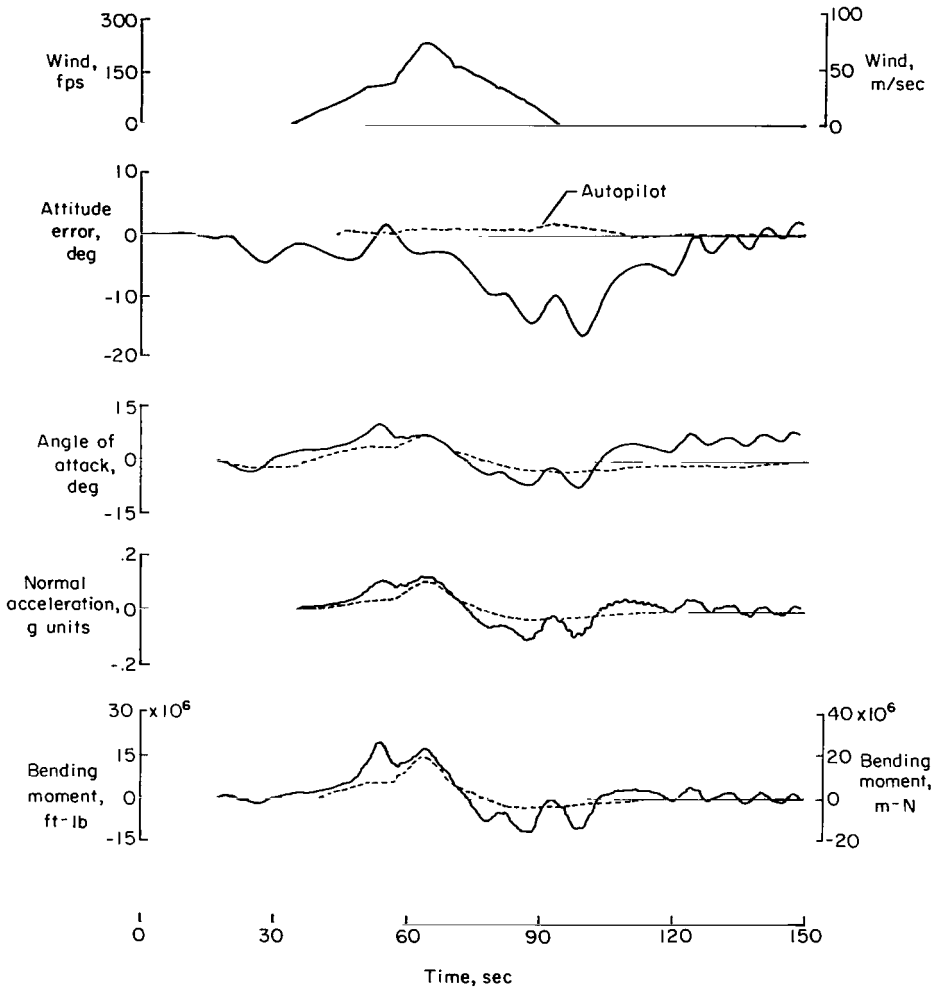

Figure 13.- Typical pitch response without augmentation.

Three Langley test pilots flew the vehicle in three control modes while encountering one of seven wind disturbances. Figure 14 shows three typical bending-moment time histories illustrating responses to wind 2 in each of the three control modes. In each case the maximum bending moment occurs at the time of peak wind velocity. The stability-augmented mode time history shows that the pilot had been supplied sufficient augmentation to reduce the bending moment to 50 percent of the bending moment when controlled by the autopilot. The rate-augmented-mode time history shows an effect of deleting the attitude feedback since the bending moment under pilot control was 75 percent of the bending moment with autopilot control. Finally, when all the augmentation is removed, the no-augmentation-mode bending-moment time history shows that the bending moment under autopilot control is exceeded by 10 percent.

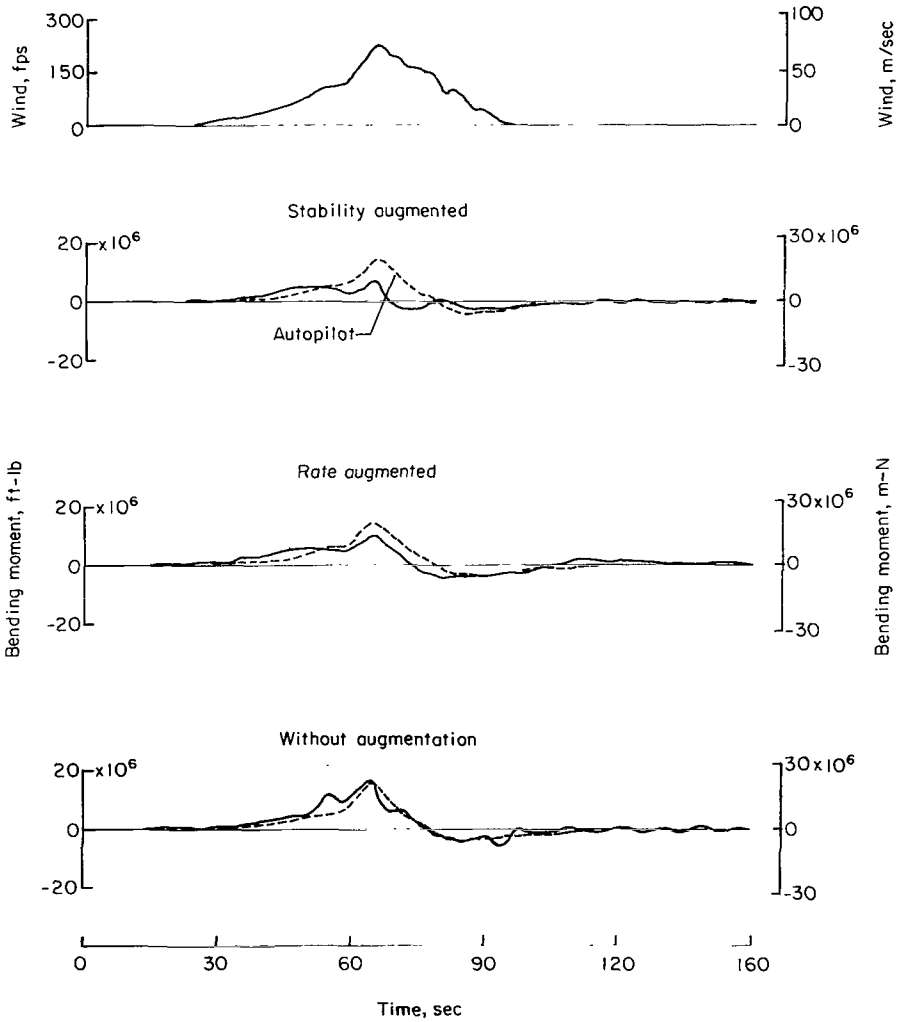

Figure 14.- Bending-moment comparison by pilot control modes.

All the maximum loads developed during simulated flights are summarized in a graphical form in figure 15. The loads have been tabulated according to the wind number; flights without a wind disturbance are designated W0, and the winds are ranked according to the maximum load developed during a flight under autopilot control. The results show little difference in the load in either the stability-augmented or rate-augmented control modes. In addition, both of these control modes resulted in significantly lower loads than with non-load-relieving autopilot control. However, when all the augmentation was removed, increased loads resulted. Indeed, the figure shows that many of the loads were double those developed during control in augmented modes. The increased loads during control in the mode without augmentation was attributed to the severity of the instability of the control system together with the display-controller lags which delay the detection of the effect of a pilot's control input.

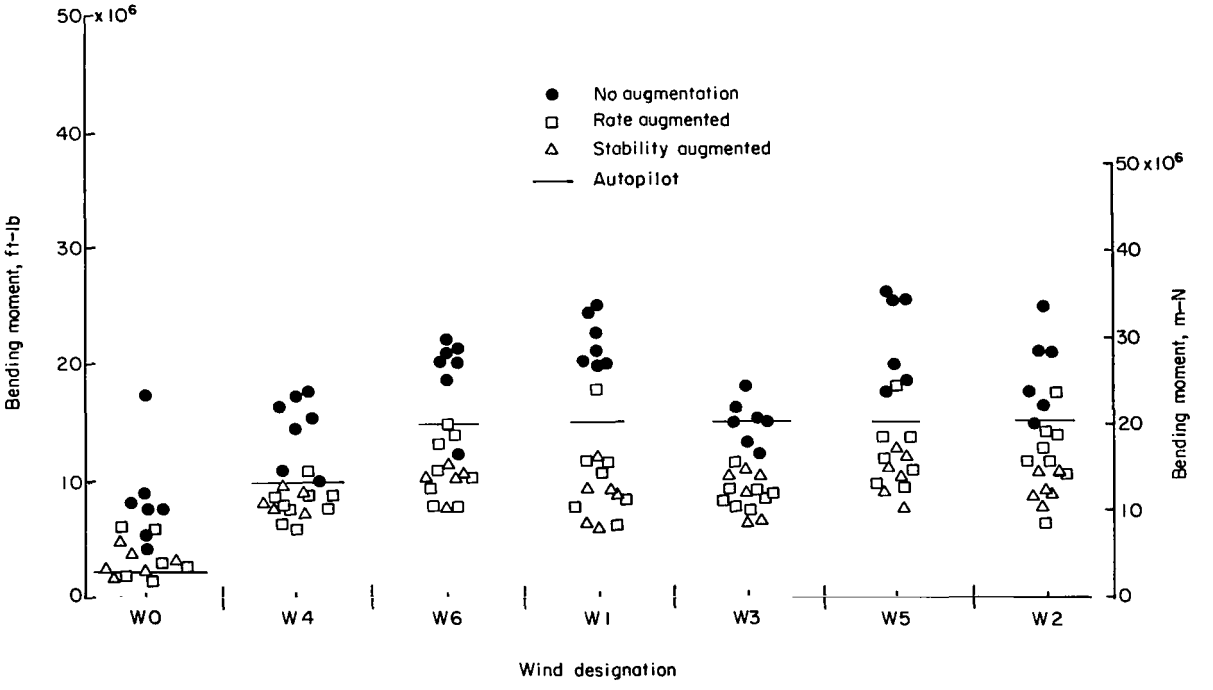

Figure 15.- Maximum bending-moment summary.

Pilot Rating

In addition to recording the piloted response, pilot ratings, according to the Cooper pilot rating schedule, were secured subsequent to each run. Thus, the rating included the pilot opinion of the control mode as well as the effect of the wind. All the pilot ratings recorded in the simulation are summarized in figure 16, according to the type of disturbing wind. Except for a few results, the ratings of the stability-augmented and rate-augmented modes are shown clustered about an average $3\frac{1}{4}$ value. However, without augmentation, the ratings jump from a barely satisfactory rating to the unsatisfactory-unacceptable region about an average value of 6, with increased scatter. This unsatisfactory rating may be attributed to the tendency for pilot's errors to accumulate in this mode and, depending on the complications, various grades of performance and rating result. In general, the effect of augmentation on the pilot ratings is shown to be similar to the effect on load. Little effect of the wind on the pilot rating is seen in the figure.

The pilots did not rate the additional roll-control task difficult and nulled the disturbance without serious effort.

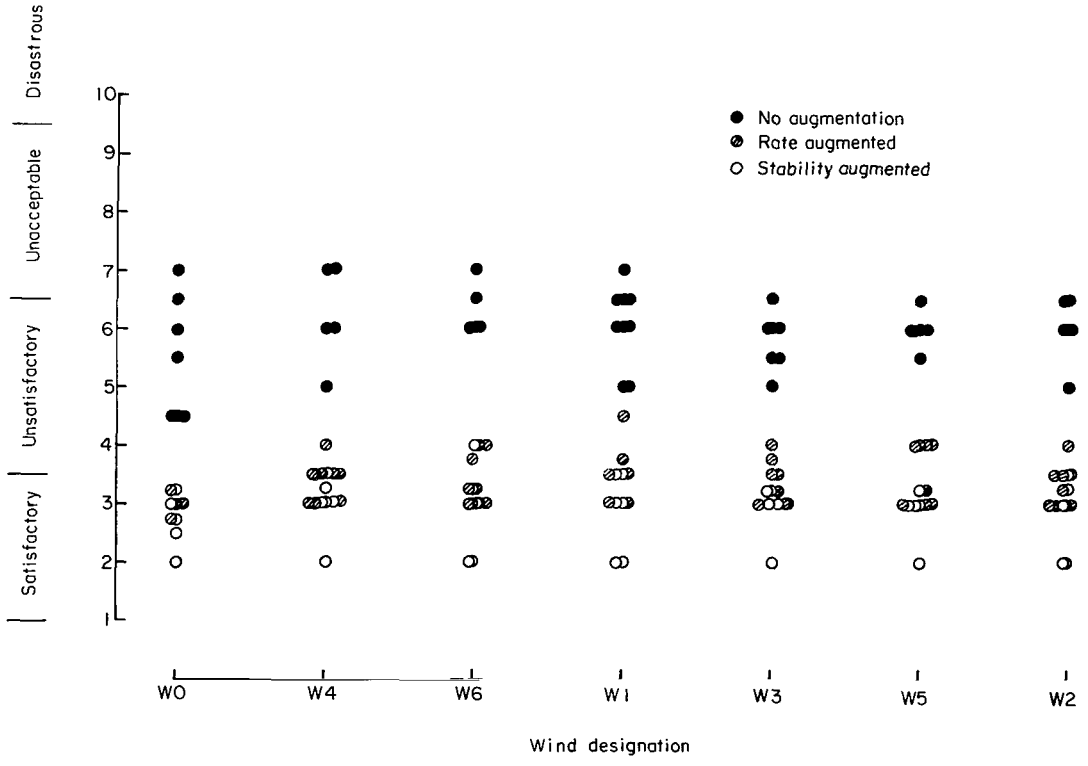

Figure 16.- Pilot ratings.

Effect of Winds

The wind profiles were considered severe by the pilots and the rapid reversal exhibited by wind 5 was considered near the limit of the pilot's ability to follow. Because these reversals were prevalent in all winds, large angles of attack due to wind were developed during the flights. Since the angle of attack (or in this case, normal acceleration) is a predominant load component, it was essential to reduce it rapidly; however, because of the inherent lag between the controller input and the resulting acceleration, care had to be exercised to prevent large excursions when reducing loads. Typical wind-induced angles of attack ranged to 10° (0.14 rad) compared with body angles of attack of 6° (0.1 rad).

CONCLUDING REMARKS

A simulator study of the loads induced on a launch vehicle while under pilot control during first-stage flight has been conducted. Three control modes were used in the study: (1) stability augmented, (2) rate augmented, and (3) no augmentation. The simulated launches were disturbed by one of six arbitrarily selected wind profiles. The maximum loads developed in the vehicle during simulated flights through these winds were compared with loads incurred by autopilot-controlled flights encountering the same winds. A total of nearly 150 simulator flights were made with test pilots controlling the vehicle.

The pilots were able to control the vehicle in each control mode and were able to hold the maximum load below that of a non-load-relieving autopilot in the two modes which contained attitude-rate augmentation. Little difference in loads or handling qualities was noticed in these modes; however, the pilot opinion favored the stability-augmented mode slightly. Without augmentation, however, loads resulted which were significantly greater than the loads developed during autopilot control. These higher loads were caused by a combination of inherent system lags and the severity of the instability of the vehicle. When control became critical, the magnitude of the load was related to the control difficulty which the pilot experienced during the high dynamic-pressure flight region. In fact, because of the difficulty in this mode, pilots rated it unacceptable. Therefore, in order to provide for pilot control of a launch vehicle without any control augmentation, the vehicle structure would need to be strengthened or launches would have to be restricted to periods of low wind disturbances.

Langley Research Center,
National Aeronautics and Space Administration,
Langley Station, Hampton, Va., November 9, 1965.

APPENDIX A

TRANSFER FUNCTIONS OF SIMULATION INSTRUMENTS

The display instruments are ideally represented as the following critically damped second-order systems. Following the transfer function, the departure from zero decibels is given as a measure of the actual characteristics of the instruments.

All-attitude indicator:

Pitch attitude (presented by sphere) –

$$\left(\frac{10.5}{s + 10.5}\right)^2, \qquad -1.4 \text{ dB at } \omega = 10.5 \text{ rad/sec}$$

Pitch command (presented by needle) –

$$\left(\frac{23.2}{s + 23.2}\right)^2, \qquad -3 \text{ dB at } \omega = 23.2 \text{ rad/sec}$$

Roll –

$$\left(\frac{8.67}{s + 8.67}\right)^2, \qquad -0.8 \text{ dB at } \omega = 8.67 \text{ rad/sec}$$

Rate meter:

Pitch accelerometer –

$$\left(\frac{19.4}{s + 19.4}\right)^2, \qquad -5.8 \text{ dB at } \omega = 19.4 \text{ rad/sec}$$

Two-Axis-Controller Characteristics

The controller has the following characteristics about each of its two usable axes:

Pitch –

Maximum displacement . . . . . $\pm 22^{\circ}$ (0.384 radian)

Spring force at maximum displacement. . . 14 oz (0.397 kg)

APPENDIX A

Roll –

Maximum displacement . . . . . ±29° (0.506 radian)

Spring force at maximum displacement. . . 18 oz (0.510 kg)

APPENDIX B

BASIC PROPERTIES OF SIMULATED VEHICLE

The basic properties of the simulated vehicle are given in the following equations:

Vehicle mass:

$$m_t = 186\,500 - 884.4t \text{ slugs} \qquad 0 \leqq t \leqq 144.45$$

$$m_t = 58\,700 - 707.5t \text{ slugs} \qquad 144.45 \leqq t \leqq 150.45$$

or

$$m_t = 2.72 \times 10^6 - 1290t \text{ kg} \qquad 0 \leqq t \leqq 144.45$$

$$m_t = 0.856 \times 10^6 - 1032t \text{ kg} \qquad 144.45 \leqq t \leqq 150.45$$

Vehicle center of mass:

$$x_{cg} = 89.53 + 0.1612t - 32.45 \times 10^{-4}\, t^2 + 30.60 \times 10^{-6}\, t^3 \text{ ft}$$

or

$$x_{cg} = 27.3 + 0.04915t - 9.9 \times 10^{-4}\, t^2 + 9.34 \times 10^{-6}\, t^3 \text{ m}$$

Bending-mode generalized mass:

$$m_q = 108\,200 - 416t \text{ slugs}$$

or

$$m_q = 1.580 \times 10^6 - 6070t \text{ kg}$$

where

$$\phi_g = 1$$

Bending-moment gradients:

$$C_{b,1} = -2.24 \times 10^6 \text{ lb-sec}^2 = -9.96 \times 10^6 \text{ N-sec}^2$$

$$C_{b,2} = -2097 \times 10^6 + 2.239 \times 10^6\, x_{cg} \text{ ft-lb-sec}^2$$

or

$$C_{b,2} = -2843 \times 10^6 + 9.96 \times 10^6\, x_{cg} \text{ m-N-sec}^2$$

$$C_{b,3} = -1.387 \times 10^6 \text{ lb-sec}^2 = -6.17 \times 10^6 \text{ N-sec}^2$$

REFERENCES

1. Nagel, R. G.; and Smith, R. E.: X-15 Pilot-in-the-Loop and Redundant/Emergency Systems Evaluation. FTC TDR 62-20, U.S. Air Force, Oct. 1962.

2. Holleman, Euclid C.; Armstrong, Neil A.; and Andrews, William H.: Utilization of the Pilot in the Launch and Injection of a Multistage Orbital Vehicle. Paper No. 60-16, Inst. Aero. Sci., Jan 25-27, 1960.

3. Space Systems Division: Titan III Flight Control System – Studies Human Pilot Capability. ER-12378, The Martin Co., Mar. 30, 1962.

4. Boeing Pibol Working Group: Pilot in the Booster Control Loop Study – Final Report (Volumes I and II). D2-80762, The Boeing Co., Dec. 1962.

5. Hardy, Gordon H.; West, James V.; and Gunderson, Robert W.: Evaluation of the Pilot's Ability to Stabilize a Flexible Launch Vehicle During First-Stage Boost. NASA TN D-2807, 1965.

6. Lester, Harold C.; and Collins, Dennis F.: Determination of Loads on a Flexible Launch Vehicle During Ascent Through Winds. NASA TN D-2590, 1965.

7. Sissenwine, Norman: Revised 1% Synthetic Wind Profile. Geophysics Research Directorate, Air Force Cambridge Research Center, June 1959. [Revision to Air Force Surveys in Geophysics No. 57 (AFCRC-TN-54-22), 1954.]

8. Smith, J. W.; and Vaughan, W. W.: Monthly and Annual Wind Distribution as a Function of Altitude for Patrick Air Force Base, Cape Canaveral, Florida. NASA TN D-610, 1961.

9. Cooper, George E.: Understanding and Interpreting Pilot Opinion. Aeron. Eng. Rev., vol. 16, no. 3, Mar. 1957, pp. 47-51, 56.

10. Bohne, Q. R.; Clingan, B. E.; deCeault, C. W.; and Deutschle, P. C.: The Dynamic Response of Advanced Vehicles. WADD Tech. Rept. 60-518, U.S. Air Force, Sept. 1960.

"The aeronautical and space activities of the United States shall be conducted so as to contribute . . . to the expansion of human knowledge of phenomena in the atmosphere and space. The Administration shall provide for the widest practicable and appropriate dissemination of information concerning its activities and the results thereof."

—NATIONAL AERONAUTICS AND SPACE ACT OF 1958

NASA SCIENTIFIC AND TECHNICAL PUBLICATIONS

TECHNICAL REPORTS: Scientific and technical information considered important, complete, and a lasting contribution to existing knowledge.

TECHNICAL NOTES: Information less broad in scope but nevertheless of importance as a contribution to existing knowledge.

TECHNICAL MEMORANDUMS: Information receiving limited distribution because of preliminary data, security classification, or other reasons.

CONTRACTOR REPORTS: Technical information generated in connection with a NASA contract or grant and released under NASA auspices.

TECHNICAL TRANSLATIONS: Information published in a foreign language considered to merit NASA distribution in English.

TECHNICAL REPRINTS: Information derived from NASA activities and initially published in the form of journal articles.

SPECIAL PUBLICATIONS: Information derived from or of value to NASA activities but not necessarily reporting the results of individual NASA-programmed scientific efforts. Publications include conference proceedings, monographs, data compilations, handbooks, sourcebooks, and special bibliographies.

Details on the availability of these publications may be obtained from:

SCIENTIFIC AND TECHNICAL INFORMATION DIVISION

NATIONAL AERONAUTICS AND SPACE ADMINISTRATION

Washington, D.C. 20546